



CHORUS

This is the accepted manuscript made available via CHORUS. The article has been published as:

Dihadron momentum imbalance and correlations in d+Au collisions

Zhong-Bo Kang, Ivan Vitev, and Hongxi Xing

Phys. Rev. D **85**, 054024 — Published 28 March 2012

DOI: [10.1103/PhysRevD.85.054024](https://doi.org/10.1103/PhysRevD.85.054024)

Dihadron momentum imbalance and correlations in d+Au collisions

Zhong-Bo Kang,^{1,*} Ivan Vitev,^{2,†} and Hongxi Xing^{3,4,‡}

¹*RIKEN BNL Research Center, Brookhaven National Laboratory, Upton, NY 11973, USA*

²*Theoretical Division, Los Alamos National Laboratory, Los Alamos, NM 87545, USA*

³*Institute of Particle Physics, Central China Normal University, Wuhan 430079, China*

⁴*Nuclear Science Division, Lawrence Berkeley National Laboratory, Berkeley, CA 94720, USA*

We calculate in perturbative QCD the transverse momentum imbalance of dijet and dihadron production in high energy p+A (d+A) collisions. We evaluate the effect of both initial- and final-state multiple scattering, which determines the strength of this transverse momentum imbalance. Combining this new result with the suppression of the cross section in d+Au collisions, which arises from cold nuclear matter energy loss and coherent power corrections, we are able to describe the dihadron correlations measured by both PHENIX and STAR collaborations at RHIC, including mid-mid, mid-forward, and forward-forward rapidity hadron pairs.

PACS numbers: 12.38.Bx, 12.39.St, 24.85.+p, 25.75.Bh

I. INTRODUCTION

In recent years, there has been renewed interest in nuclear effects that affect hadronic observables in proton-nucleus (p+A) and deuteron-nucleus (d+A) collisions [1]. Much of this interest was sparked by forward rapidity measurements in d+Au collisions at the Relativistic Heavy Ion Collider (RHIC) that indicate considerable suppression of both single hadron and dihadron production cross sections relative to the binary collision scaled proton-proton (p+p) baseline [2–6]. Back-to-back dihadron correlation measurements have attracted the most attention and are under active investigation in the framework of different theoretical formalisms [7–11]. On one hand, quantifying the differences between p+A (d+A) and p+p collisions (referred to as “cold nuclear matter effects”) can provide a solid baseline for the unambiguous identification of any additional final-state hot and dense medium effects in heavy ion collisions [12]. On the other hand, the study of p+A (d+A) collisions at forward rapidity is interesting in its own right since it probes the inelastic and coherent multiple parton scattering in the nucleus, as well as any possible modification of the small- x parton distribution functions [7–11, 13–16].

In perturbative QCD, at leading order, high transverse momentum (p_{\perp}) particle production arises from hard $2 \rightarrow 2$ scattering processes. In this picture, two incoming collinear partons scatter on each other to produce two high transverse momentum partons, which then fragment into jets of hadrons. These jets, as well as the hadron pair formed by their leading particles, are approximately back-to-back in the transverse plane. In high energy proton-nucleus reactions the incoming partons that participate in the collision can undergo multiple interactions. Even in the presence of multiple parton scattering, particle production at high transverse momentum is dominated by a single hard interaction $Q^2 \propto p_{\perp}^2 \gg \xi^2$, where ξ^2 is the typical scale of the soft transverse momentum exchanges. We refer to the interactions that precede the large Q^2 scattering as initial-state and the interactions that follow the large Q^2 scattering as final-state.

Both initial- and final-state multiple interactions can affect dijet (dihadron) production in p+A (d+A) reactions. More specifically, they lead to an increase in the transverse momentum imbalance [17] that can be perturbatively computed within a high-twist formalism [16–18]. In this paper we give a theoretical derivation of the increase in the transverse momentum imbalance and demonstrate that it will lead to a broader away-side peak for the dihadron azimuthal correlation distribution in d+A collisions, consistent with the experimental observations at RHIC. Furthermore, multiple parton scattering also manifests itself through medium-induced radiative corrections [19, 20] and power suppressed contribution to the cross sections. In reactions with nuclei (p+A and A+A) initial-state radiative energy loss effects are always present but their effect is most pronounced at forward rapidity [13, 21]. In the coherent scattering regime, the high-twist contributions are enhanced by the nuclear-size $\propto A^{1/3}$ and may become important at small and moderate transverse momenta. Such nuclear-size enhanced power corrections have been resummed for both inclusive single hadron and dihadron production processes in p+A collisions [7]. In the phenomenological part of this paper we combine the broadening in the away-side width with the nuclear cross section suppression to study the

* zkang@bnl.gov

† ivitev@lanl.gov

‡ xinghx@iopp.cnu.edu.cn

modification of the production rate and observed shape of dihadron azimuthal correlations in going from p+p to p+A (d+A) collisions. With parton scattering parameters in cold nuclear matter constrained by deep inelastic scattering experiments [22], calculations are consistent with the experimental measurements at RHIC [5, 6].

The rest of our paper is organized as follows: in Sec. II we take into account both initial- and final-state multiple parton scattering to calculate the increase in the transverse momentum imbalance of dijet and dihadron production in p+A (d+A) collisions. In Sec. III we first evaluate the width of the away-side peak of the dihadron correlation distribution at RHIC and show that our formalism can describe the PHENIX experimental data well if we take into account the nuclear-induced increase in the transverse momentum imbalance. We then overview the nuclear effects that lead to the suppression of single and double inclusive hadron production in p+A (d+A) reactions. We demonstrate that the calculated mid-forward and forward-forward rapidity hadron pair production attenuation is consistent with recent PHENIX measurements. At the end of this section, by combining the nuclear suppression and the increase in the transverse momentum imbalance, we are able to describe the dihadron azimuthal correlation distribution observed by the STAR experiment at RHIC. Summary and conclusions are presented in Sec. IV.

II. DIJET AND DIHADRON TRANSVERSE MOMENTUM IMBALANCE IN $p + A$ COLLISIONS

In this section we derive the increase in the transverse momentum imbalance of back-to-back jet production in p+A collisions. This phenomenon is often referred to as nuclear-induced broadening in the literature. We then generalize the formalism to study back-to-back hadron production.

A. Dijet transverse momentum imbalance

We start by describing the pQCD formalism for evaluating dijet production in p+p collisions:

$$p(P') + p(P) \rightarrow J_1(P_{1\perp}) + J_2(P_{2\perp}) + X. \quad (1)$$

Let us define $P_{\perp} = |\vec{P}_{1\perp} - \vec{P}_{2\perp}|/2$ to be the magnitude of the average transverse momentum of the jet pair. In leading order perturbative QCD, the jets are produced back-to-back, $\vec{P}_{1\perp} = -\vec{P}_{2\perp}$, thus $|\vec{P}_{1\perp}| = |\vec{P}_{2\perp}| = P_{\perp}$. The differential cross section can be written as [23]:

$$\frac{d\sigma}{dy_1 dy_2 dP_{\perp}^2} = \frac{\pi\alpha_s^2}{s^2} \sum_{a,b} \frac{f_{a/p}(x') f_{b/p}(x)}{x'x} H_{ab \rightarrow cd}^U(\hat{s}, \hat{t}, \hat{u}), \quad (2)$$

where $\sum_{a,b}$ runs over all parton flavors, $s = (P' + P)^2$, $f_{a,b/p}(x)$ are the parton distribution functions with the momentum fractions $x' = \frac{P_{\perp}}{\sqrt{s}}(e^{y_1} + e^{y_2})$, $x = \frac{P_{\perp}}{\sqrt{s}}(e^{-y_1} + e^{-y_2})$, and y_1, y_2 the rapidities of the two jets. $H_{ab \rightarrow cd}^U(\hat{s}, \hat{t}, \hat{u})$ are the partonic cross sections as a function of the usual partonic Mandelstam variables $\hat{s}, \hat{t}, \hat{u}$. These cross sections are well-known [23], we will reproduce them here for later convenience:

$$H_{qq' \rightarrow qq'}^U = \frac{N_c^2 - 1}{2N_c^2} \left[\frac{\hat{s}^2 + \hat{u}^2}{\hat{t}^2} \right], \quad (3)$$

$$H_{qq \rightarrow qq}^U = \frac{N_c^2 - 1}{2N_c^2} \left[\frac{\hat{s}^2 + \hat{u}^2}{\hat{t}^2} + \frac{\hat{s}^2 + \hat{t}^2}{\hat{u}^2} \right] - \frac{N_c^2 - 1}{N_c^3} \left[\frac{\hat{s}^2}{\hat{t}\hat{u}} \right], \quad (4)$$

$$H_{q\bar{q} \rightarrow q'\bar{q}'}^U = \frac{N_c^2 - 1}{2N_c^2} \left[\frac{\hat{t}^2 + \hat{u}^2}{\hat{s}^2} \right], \quad (5)$$

$$H_{q\bar{q} \rightarrow q\bar{q}}^U = \frac{N_c^2 - 1}{2N_c^2} \left[\frac{\hat{t}^2 + \hat{u}^2}{\hat{s}^2} + \frac{\hat{s}^2 + \hat{u}^2}{\hat{t}^2} \right] - \frac{N_c^2 - 1}{N_c^3} \left[\frac{\hat{u}^2}{\hat{s}\hat{t}} \right], \quad (6)$$

$$H_{qg \rightarrow qg}^U = -\frac{N_c^2 - 1}{2N_c^2} \left[\frac{\hat{s}}{\hat{u}} + \frac{\hat{u}}{\hat{s}} \right] + \left[\frac{\hat{s}^2 + \hat{u}^2}{\hat{t}^2} \right], \quad (7)$$

$$H_{q\bar{q} \rightarrow gg}^U = \frac{(N_c^2 - 1)^2}{2N_c^3} \left[\frac{\hat{t}}{\hat{u}} + \frac{\hat{u}}{\hat{t}} \right] - \frac{N_c^2 - 1}{N_c} \left[\frac{\hat{t}^2 + \hat{u}^2}{\hat{s}^2} \right], \quad (8)$$

$$H_{gg \rightarrow q\bar{q}}^U = \frac{1}{2N_c} \left[\frac{\hat{t}}{\hat{u}} + \frac{\hat{u}}{\hat{t}} \right] - \frac{N_c}{N_c^2 - 1} \left[\frac{\hat{t}^2 + \hat{u}^2}{\hat{s}^2} \right], \quad (9)$$

$$H_{gg \rightarrow gg}^U = \frac{4N_c^2}{N_c^2 - 1} \left[3 - \frac{\hat{t}\hat{u}}{\hat{s}^2} - \frac{\hat{s}\hat{u}}{\hat{t}^2} - \frac{\hat{s}\hat{t}}{\hat{u}^2} \right], \quad (10)$$

where $N_c = 3$ is the number of colors.

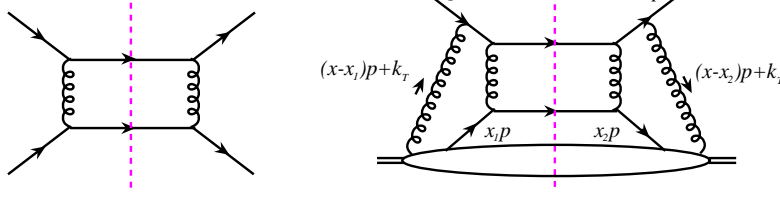


FIG. 1. Left: Feynman diagram for the partonic $qq' \rightarrow qq'$ scattering channel. Right: initial-state double scattering Feynman diagram that contributes to the dijet transverse momentum imbalance increase.

Let us now study dijet production in proton-nucleus collisions. In such collisions the energetic incoming parton from the proton can undergo multiple scattering with the soft partons inside the nuclear matter before the hard collisions. We refer to these interactions as initial-state multiple scattering. After the hard collisions, the two leading partons, produced almost back-to-back, will eventually hadronize into jets as observed in the experiments. However, these partons will also likely undergo multiple interactions in the large nucleus. We refer to these interactions as final-state multiple scattering. Such separation is only possible when the scale of hard scattering is considerably larger than the scale of typical transverse momentum exchanges between the projectile and the medium, $Q^2 \gg \xi^2$ [21]. The initial- and final-state multiple scattering lead to dijet acoplanarity, or imbalance. To quantify this effect, let us define the dijet transverse momentum imbalance \vec{q}_\perp as:

$$\vec{q}_\perp = \vec{P}_{1\perp} + \vec{P}_{2\perp}, \quad (11)$$

and the averaged transverse momentum imbalance square as:

$$\langle q_\perp^2 \rangle = \int d^2\vec{q}_\perp q_\perp^2 \frac{d\sigma}{dy_1 dy_2 dP_\perp^2 d^2\vec{q}_\perp} \bigg/ \frac{d\sigma}{dy_1 dy_2 dP_\perp^2}. \quad (12)$$

The nuclear enhancement (or broadening) of the transverse momentum imbalance in p+A collisions relative to p+p collisions can be quantified by the difference:

$$\Delta\langle q_\perp^2 \rangle = \langle q_\perp^2 \rangle_{pA} - \langle q_\perp^2 \rangle_{pp}. \quad (13)$$

As demonstrated in Ref. [16], the transverse momentum imbalance increase $\Delta\langle q_\perp^2 \rangle$ can be calculated perturbatively and the leading contribution comes from double scattering. To illustrate the method, we will study the simple partonic channel $qq' \rightarrow qq'$. At lowest order, the partonic cross section $H_{qq' \rightarrow qq'}^U$ is calculated from the Feynman diagram in Fig. 1 (left). At this order, the transverse momenta of the two outgoing partons (or the dijet) are equal and opposite and we have:

$$\frac{d\sigma}{dy_1 dy_2 dP_\perp^2 d^2\vec{q}_\perp} \propto \delta^2(\vec{q}_\perp). \quad (14)$$

The leading contribution to the transverse momentum imbalance increase in p+A collisions comes from either initial-state double scattering, as in Fig. 1 (right); or final-state double scattering, as in Fig. 2. Let us first focus on the calculation of initial-state double scattering. In this case, the small k_\perp -kick in the nucleus will generate a small transverse momentum imbalance for the dijet:

$$\vec{q}_\perp = \vec{P}_{1\perp} + \vec{P}_{2\perp} = \vec{k}_\perp. \quad (15)$$

Following [16], we evaluate the contribution from the double scattering diagram to $\langle q_\perp^2 \rangle_{pA}$:

$$\int d^2\vec{q}_\perp q_\perp^2 \frac{d\sigma_{pA}}{dy_1 dy_2 dP_\perp^2 d^2\vec{q}_\perp} = \frac{\pi\alpha_s^2}{s^2} \frac{f_{q/p}(x')}{x'x} \int d^2\vec{q}_\perp q_\perp^2 \int dx_1 dx_2 d^2k_\perp \bar{T}_{Aq}(x, x_1, x_2, k_\perp) \times \bar{H}(x, x_1, x_2, k_\perp, x'p') \delta^2(\vec{q}_\perp - \vec{k}_\perp), \quad (16)$$

where the matrix element \bar{T}_{Aq} is represented by the bottom blob in Fig. 1 (right) and has the following expression:

$$\bar{T}_{Aq}(x, x_1, x_2, k_\perp) = \int \frac{dy^-}{2\pi} \frac{dy_1^-}{2\pi} \frac{dy_2^-}{2\pi} \int \frac{d^2y_\perp}{(2\pi)^2} e^{ix_1 p^+ y_1^-} e^{i(x-x_1)p^+ y^-} e^{-i(x-x_2)p^+ y_2^-} e^{-ik_\perp \cdot y_\perp} \times \frac{1}{2} \langle p_A | A^+(y_2^-, 0_\perp) \bar{\psi}(0) \gamma^+ \psi(y_1^-) A^+(y^-, y_\perp) | p_A \rangle. \quad (17)$$

As in [16, 17], the calculation first takes advantage of $\delta^2(\vec{q}_\perp - \vec{k}_\perp)$ to set $q_\perp^2 = k_\perp^2$. These two factors of k_\perp can be converted into transverse derivatives on the two fields A^+ in matrix element \overline{T}_{Aq} in Eq. (17) by performing a partial integration for d^2y_\perp :

$$k_\perp^2 A^+(y_2^-, 0_\perp) A^+(y^-, y_\perp) \rightarrow F_\alpha^+(y_2^-, 0_\perp) F^{+\alpha}(y^-, y_\perp). \quad (18)$$

We then expand in k_\perp in the partonic part \overline{H} around $k_\perp^2 = 0$, and keep the first non-vanishing term:

$$H(x, x_1, x_2, x'p') \equiv \overline{H}(x, x_1, x_2, k_\perp = 0, x'p'). \quad (19)$$

In other words, since the A^+ fields have been converted to the gauge-covariant gluon field strength in the matrix element \overline{T}_{Aq} , one can set $k_\perp = 0$ in the hard part. One will later find that all such hard-parts $H(x, x_1, x_2, x'p')$ for the double scattering diagrams reduce to the lowest order Born diagrams up to color factors. Thus, the calculation of transverse momentum imbalance enhancement $\Delta\langle q_\perp^2 \rangle$ is simpler than the usual higher-twist calculations in which one calculates the multiple scattering contribution to the differential cross section itself directly (instead of the q_\perp^2 -weighted one).

We obtain:

$$\int d^2\vec{q}_\perp q_\perp^2 \frac{d\sigma_{pA}}{dy_1 dy_2 dP_\perp^2 d^2\vec{q}_\perp} = \frac{\pi\alpha_s^2}{s^2} \frac{f_{q/p}(x')}{x'x} \int dx_1 dx_2 T_{Fq}(x, x_1, x_2) H(x, x_1, x_2, x'p'), \quad (20)$$

where T_{Fq} is a twist-4 four-parton correlation function:

$$T_{Fq}^{(I)}(x, x_1, x_2) = \int \frac{dy^-}{2\pi} \frac{dy_1^-}{2\pi} \frac{dy_2^-}{2\pi} e^{ix_1 p^+ y_1^-} e^{i(x-x_1)p^+ y^-} e^{-i(x-x_2)p^+ y_2^-} \frac{1}{2} \langle p_A | F_\alpha^+(y_2^-) \bar{\psi}(0) \gamma^+ \psi(y_1^-) F^{+\alpha}(y^-) | p_A \rangle. \quad (21)$$

Here and thereafter we will use the superscript ‘‘I’’ (‘‘F’’) to indicate the contribution associated with initial- (final-) state multiple scattering. The hard partonic function $H(x, x_1, x_2, x'p')$ is given by:

$$H(x, x_1, x_2, x'p') = 8\pi^2 \alpha_s \frac{C_F}{N_c^2 - 1} \left[\frac{1}{2\pi} \frac{1}{x_1 - x - i\epsilon} \frac{1}{x_2 - x + i\epsilon} \right] H_{qq' \rightarrow qq'}^U, \quad (22)$$

where $C_F = (N_c^2 - 1)/2N_c$. Substituting Eq. (22) into Eq. (20) and performing the integration over x_1 and x_2 , we obtain:

$$\int d^2\vec{q}_\perp q_\perp^2 \frac{d\sigma_{pA}}{dy_1 dy_2 dP_\perp^2 d^2\vec{q}_\perp} = \left(\frac{8\pi^2 \alpha_s}{N_c^2 - 1} \right) \frac{\pi\alpha_s^2}{s^2} \frac{f_{q/p}(x')}{x'x} T_{q/A}^{(I)}(x) H_{qq' \rightarrow qq'}^I(\hat{s}, \hat{t}, \hat{u}), \quad (23)$$

where $T_{q/A}^{(I)}(x)$ is the twist-4 quark-gluon correlation function defined as [16, 17]:

$$T_{q/A}^{(I)}(x) = \int \frac{dy^-}{2\pi} e^{ixp^+ y^-} \int \frac{dy_1^- dy_2^-}{2\pi} \theta(y^- - y_1^-) \theta(-y_2^-) \frac{1}{2} \langle p_A | F_\alpha^+(y_2^-) \bar{\psi}_q(0) \gamma^+ \psi_q(y^-) F^{+\alpha}(y_1^-) | p_A \rangle, \quad (24)$$

and $H_{qq' \rightarrow qq'}^I$ is the hard-part function given by:

$$H_{qq' \rightarrow qq'}^I = C_F H_{qq' \rightarrow qq'}^U. \quad (25)$$

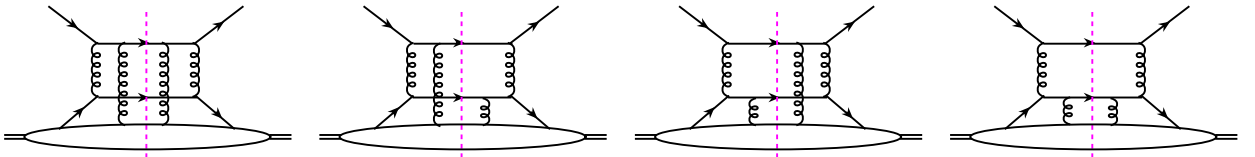


FIG. 2. Final-state double scattering Feynman diagrams that contribute to the dijet transverse momentum imbalance increase, for the partonic channel $qq' \rightarrow qq'$.

Next, we calculate the contribution to the transverse momentum imbalance from the final-state double scattering diagrams in Fig. 2. This evaluation is slightly more complicated since there are four diagrams as opposed to a single diagram for the initial-state case. However, the calculation is very similar and straightforward. Different Feynman

diagrams only differ in terms of color factors and their sum provides a measure of the average square transverse field strength probed by the outgoing partons [17]. We obtain:

$$\int d^2\vec{q}_\perp q_\perp^2 \frac{d\sigma_{pA}}{dy_1 dy_2 dP_\perp^2 d^2\vec{q}_\perp} = \left(\frac{8\pi^2\alpha_s}{N_c^2 - 1} \right) \frac{\pi\alpha_s^2}{s^2} \frac{f_{q/p}(x')}{x'x} T_{q/A}^{(F)}(x) H_{qq' \rightarrow qq'}^F(\hat{s}, \hat{t}, \hat{u}), \quad (26)$$

where $T_{q/A}^{(F)}$ is given by the same expressions in Eq. (24), except for the θ -functions that are replaced as follows [16, 17]:

$$\theta(y^- - y_1^-) \theta(-y_2^-) \rightarrow \theta(y_1^- - y^-) \theta(y_2^-), \quad (27)$$

and the final-state hard-part function H^F is given by

$$H_{qq' \rightarrow qq'}^F = \frac{(N_c^2 - 3)(N_c^2 - 1)}{2N_c^3} \left[\frac{\hat{s}^2 + \hat{u}^2}{\hat{t}^2} \right]. \quad (28)$$

Likewise, we can go ahead to calculate the contribution to the transverse momentum imbalance from both initial- and final-state double scattering diagrams for all partonic channels. The calculation is straightforward though tedious, the result can be summarized as:

$$\int d^2\vec{q}_\perp q_\perp^2 \frac{d\sigma_{pA}}{dy_1 dy_2 dP_\perp^2 d^2\vec{q}_\perp} = \left(\frac{8\pi^2\alpha_s}{N_c^2 - 1} \right) \frac{\pi\alpha_s^2}{s^2} \sum_{a,b} \frac{f_{a/p}(x')}{x'x} \left[T_{b/A}^{(I)}(x) H_{ab \rightarrow cd}^I(\hat{s}, \hat{t}, \hat{u}) + T_{b/A}^{(F)}(x) H_{ab \rightarrow cd}^F(\hat{s}, \hat{t}, \hat{u}) \right], \quad (29)$$

where $T_{q/A}^{(I,F)}(x)$ are given in Eqs. (24) and (27). In the calculation for the partonic channels $qg \rightarrow qg$ and $gg \rightarrow gg$, see for example the Feynman diagrams shown in Fig. 3, two other similar twist-4 gluon-gluon correlation functions $T_{g/A}^{(I,F)}(x)$ appear. The operator definition of $T_{g/A}^{(I)}(x)$ is given by [16, 17]:

$$T_{g/A}^{(I)}(x) = \int \frac{dy^-}{2\pi} e^{ixp^+ y^-} \int \frac{dy_1^- dy_2^-}{2\pi} \theta(y^- - y_1^-) \theta(-y_2^-) \frac{1}{xp^+} \langle p_A | F_\alpha^+(y_2^-) F^{\sigma+}(0) F_\sigma^+(y^-) F^{+\alpha}(y_1^-) | p_A \rangle, \quad (30)$$

while $T_{g/A}^{(F)}(x)$ is given by the same expression with the θ -function replacement specified in Eq. (27).

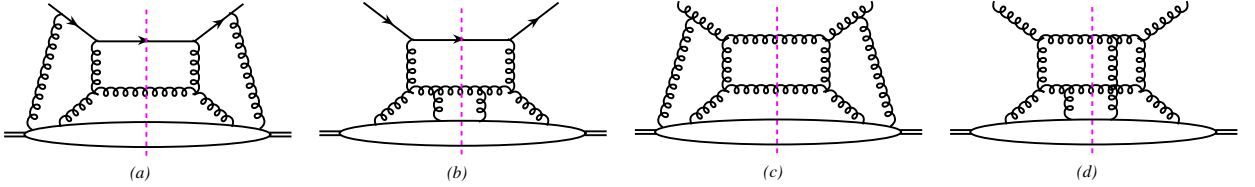


FIG. 3. Sample diagrams that contribute to the dijet transverse momentum imbalance for the partonic channels $qg \rightarrow qg$ (left two) and $gg \rightarrow gg$ (right two), where (a) and (c) are for initial-state double scattering, (b) and (d) are for final-state double scattering.

Finally, from Eqs. (2) and (29), we obtain the transverse momentum imbalance increase $\Delta\langle q_\perp^2 \rangle$ in pA collisions:

$$\Delta\langle q_\perp^2 \rangle = \left(\frac{8\pi^2\alpha_s}{N_c^2 - 1} \right) \frac{\sum_{a,b} \frac{f_{a/p}(x')}{x'x} \left[T_{b/A}^{(I)}(x) H_{ab \rightarrow cd}^I(\hat{s}, \hat{t}, \hat{u}) + T_{b/A}^{(F)}(x) H_{ab \rightarrow cd}^F(\hat{s}, \hat{t}, \hat{u}) \right]}{\sum_{a,b} \frac{f_{a/p}(x') f_{b/p}(x)}{x'x} H_{ab \rightarrow cd}^U(\hat{s}, \hat{t}, \hat{u})}. \quad (31)$$

The partonic hard-part functions $H_{ab \rightarrow cd}^I$ are associated with the initial-state multiple scattering, and are given by:

$$H_{ab \rightarrow cd}^I = \begin{cases} C_F H_{ab \rightarrow cd}^U & \text{a=quark} \\ C_A H_{ab \rightarrow cd}^U & \text{a=gluon} \end{cases}, \quad (32)$$

with $C_A = N_c$. On the other hand, $H_{ab \rightarrow cd}^F$ are associated with the final-state multiple scattering, and are given by:

$$H_{qq' \rightarrow qq'}^F = \frac{(N_c^2 - 3)(N_c^2 - 1)}{2N_c^3} \left[\frac{\hat{s}^2 + \hat{u}^2}{\hat{t}^2} \right], \quad (33)$$

$$H_{qq \rightarrow qq}^F = \frac{(N_c^2 - 3)(N_c^2 - 1)}{2N_c^3} \left[\frac{\hat{s}^2 + \hat{u}^2}{\hat{t}^2} + \frac{\hat{s}^2 + \hat{t}^2}{\hat{u}^2} \right] + \frac{2(N_c^2 - 1)}{N_c^4} \left[\frac{\hat{s}^2}{\hat{t}\hat{u}} \right], \quad (34)$$

$$H_{q\bar{q} \rightarrow q'\bar{q}'}^F = C_A H_{q\bar{q} \rightarrow q'\bar{q}'}^U, \quad (35)$$

$$H_{q\bar{q} \rightarrow q\bar{q}}^F = C_A H_{q\bar{q} \rightarrow q\bar{q}}^U - \frac{(N_c^2 - 1)^2}{2N_c^3} \left[\frac{\hat{s}^2 + \hat{u}^2}{\hat{t}^2} \right], \quad (36)$$

$$H_{qg \rightarrow qg}^F = C_F H_{qg \rightarrow qg}^U - \frac{N_c}{2} \left[\frac{\hat{s}(\hat{s}^2 + \hat{u}^2)}{\hat{t}^2 \hat{u}} \right], \quad (37)$$

$$H_{q\bar{q} \rightarrow gg}^F = C_A H_{q\bar{q} \rightarrow gg}^U - \frac{N_c^2 - 1}{2N_c^2} \left[\frac{\hat{t}}{\hat{u}} + \frac{\hat{u}}{\hat{t}} \right], \quad (38)$$

$$H_{gg \rightarrow q\bar{q}}^F = C_A H_{gg \rightarrow q\bar{q}}^U - \frac{1}{2(N_c^2 - 1)} \left[\frac{\hat{t}}{\hat{u}} + \frac{\hat{u}}{\hat{t}} \right], \quad (39)$$

$$H_{gg \rightarrow gg}^F = C_A H_{gg \rightarrow gg}^U + \frac{2N_c^3}{(N_c^2 - 1)^2} \left[\frac{\hat{t}}{\hat{u}} + \frac{\hat{u}}{\hat{t}} + 1 \right]^2. \quad (40)$$

B. Dihadron transverse momentum imbalance

One can easily generalize the transverse momentum imbalance for dijet production to dihadron production. To start, we write down the leading order differential cross section for dihadron production in p+p collisions, $p(P') + p(P) \rightarrow h_1(p_{1\perp}) + h_2(p_{2\perp}) + X$,

$$\frac{d\sigma}{dy_1 dy_2 dp_{1\perp} dp_{2\perp}} = \frac{2\pi\alpha_s^2}{s^2} \sum_{abcd} \int \frac{dz_1}{z_1} D_{h_1/c}(z_1) D_{h_2/d}(z_2) \frac{f_{a/p}(x') f_{b/p}(x)}{x'x} H_{ab \rightarrow cd}^U(\hat{s}, \hat{t}, \hat{u}), \quad (41)$$

where $D_{h_1/c}(z_1)$ and $D_{h_2/d}(z_2)$ are fragmentation functions, $z_2 = z_1 p_{2\perp}/p_{1\perp}$ [13], and:

$$x' = \frac{p_{1\perp}}{z_1 \sqrt{s}} (e^{y_1} + e^{y_2}), \quad x = \frac{p_{1\perp}}{z_1 \sqrt{s}} (e^{-y_1} + e^{-y_2}). \quad (42)$$

At this order, the final hadron pair comes from the fragmentation of the back-to-back parton pair in the partonic collision $ab \rightarrow cd$. One has $\vec{p}_{1\perp} = z_1 \vec{P}_\perp$ and $\vec{p}_{2\perp} = -z_2 \vec{P}_\perp$ with \vec{P}_\perp the transverse momentum of the first parent parton. Then, the dihadron transverse momentum imbalance \vec{q}_\perp can be written as:

$$\vec{q}_\perp \equiv \vec{p}_{1\perp} + \vec{p}_{2\perp} = (z_1 - z_2) \vec{P}_\perp. \quad (43)$$

Thus, the averaged transverse momentum imbalance $\langle q_\perp^2 \rangle$ in p+p collisions is:

$$\langle q_\perp^2 \rangle_{pp} = \int d^2 \vec{q}_\perp q_\perp^2 \frac{d\sigma}{dy_1 dy_2 dp_{1\perp} dp_{2\perp} d^2 \vec{q}_\perp} / \frac{d\sigma}{dy_1 dy_2 dp_{1\perp} dp_{2\perp}} \sim \langle (z_1 - z_2)^2 P_\perp^2 \rangle. \quad (44)$$

On the other hand, in p+A collisions there will be transverse momentum imbalance increase generated by the small k_\perp -kick from the initial- and final-state multiple scattering in the nuclear medium, as demonstrated in the previous section. Since the two effects are independent:

$$\langle q_\perp^2 \rangle_{pA} = \langle ((z_1 - z_2) \vec{P}_\perp + \vec{k}_\perp)^2 \rangle = \langle (z_1 - z_2)^2 P_\perp^2 \rangle + \langle k_\perp^2 \rangle, \quad (45)$$

where in the second step we have taken $\langle (z_1 - z_2) \vec{P}_\perp \cdot \vec{k}_\perp \rangle = 0$ due to the random nature of the k_\perp -kick. Thus, the transverse momentum imbalance increase in p+A collisions when compared to p+p collisions is given by:

$$\Delta \langle q_\perp^2 \rangle = \langle q_\perp^2 \rangle_{pA} - \langle q_\perp^2 \rangle_{pp} = \langle k_\perp^2 \rangle, \quad (46)$$

and is equal to the strength of the soft k_\perp -kick from the multiple scattering. From the result of the last section, we immediately obtain for the dihadron production:

$$\Delta \langle q_\perp^2 \rangle = \left(\frac{8\pi^2 \alpha_s}{N_c^2 - 1} \right) \frac{\sum_{abcd} \int \frac{dz_1}{z_1} D_{h_1/c}(z_1) D_{h_2/d}(z_2) \frac{f_{a/p}(x')}{x'x} \left[T_{b/A}^{(I)}(x) H_{ab \rightarrow cd}^I(\hat{s}, \hat{t}, \hat{u}) + T_{b/A}^{(F)}(x) H_{ab \rightarrow cd}^F(\hat{s}, \hat{t}, \hat{u}) \right]}{\sum_{abcd} \int \frac{dz_1}{z_1} D_{h_1/c}(z_1) D_{h_2/d}(z_2) \frac{f_{a/p}(x') f_{b/p}(x)}{x'x} H_{ab \rightarrow cd}^U(\hat{s}, \hat{t}, \hat{u})}. \quad (47)$$

Eqs. (31) and (47) are the main new theoretical results of our paper. We will use them in the phenomenological studies of dihadron azimuthal correlations in the next section.

III. DIHADRON CORRELATION IN $d + Au$ COLLISIONS

In this section, we study the phenomenological applications of our results. First, we use the transverse momentum imbalance result to derive the width of the away-side peak in dihadron correlations and compare our findings to existing experimental data. Next, we review the nuclear effects which lead to the suppression of dihadron production in $d+Au$ collisions and calculate the nuclear modification factor $R_{dA}^{(2)}$, which turns out to describe the data reasonably well. Finally combining the calculation on both the away-side width and the nuclear suppression factor, we are able to describe the broadening of the dihadron azimuthal correlations in $d+Au$ collisions relative to $p+p$ collisions.

A. Dihadron imbalance and the width of the away-side peak

In order to estimate the nuclear-induced broadening for dihadron production given by Eq. (47), one needs to know the four-parton correlation functions $T_{b/A}^{(I,F)}(x)$ with $b = q, g$. Following Refs. [7, 22], these can be modeled as:

$$\frac{4\pi^2\alpha_s}{N_c} T_{q,g/A}^{(I)}(x) = \frac{4\pi^2\alpha_s}{N_c} T_{q,g/A}^{(F)}(x) = \xi^2 \left(A^{1/3} - 1 \right) f_{q,g/A}(x). \quad (48)$$

Such decomposition into a leading twist parton distribution function and nuclear enhanced transverse momentum transfers squared and/or power corrections is motivated by the θ -function structure, and the similarity of the operator definition between $T_{q,g/A}^{(I,F)}(x)$ and $f_{q,g/A}(x)$. In Eq. (48) $\xi^2 = 0.09 - 0.12 \text{ GeV}^2$ represents a characteristic scale of high twist corrections per nucleon and has been extracted from deep inelastic scattering data [22]. It has also been employed to describe single inclusive hadron production in $d+Au$ collisions at forward rapidities [7, 13, 21]. We can now write the increase of transverse momentum imbalance as:

$$\Delta\langle q_{\perp}^2 \rangle = \frac{2N_c}{N_c^2 - 1} \xi^2 \left(A^{1/3} - 1 \right) \frac{\sum_{abcd} \int \frac{dz_1}{z_1} D_{h_1/c}(z_1) D_{h_2/d}(z_2) \frac{f_{a/p}(x') f_{b/A}(x)}{x'x} [H_{ab \rightarrow cd}^I(\hat{s}, \hat{t}, \hat{u}) + H_{ab \rightarrow cd}^F(\hat{s}, \hat{t}, \hat{u})]}{\sum_{abcd} \int \frac{dz_1}{z_1} D_{h_1/c}(z_1) D_{h_2/d}(z_2) \frac{f_{a/p}(x') f_{b/p}(x)}{x'x} H_{ab \rightarrow cd}^U(\hat{s}, \hat{t}, \hat{u})}. \quad (49)$$

The transverse momentum imbalance $\langle q_{\perp}^2 \rangle_{dA} = \langle q_{\perp}^2 \rangle_{pp} + \Delta\langle q_{\perp}^2 \rangle$ characterizes the shape of the azimuthal correlation of back-to-back dihadron production in $d+Au$ collisions, as it is closely related to the width of the away-side peak σ_F . First, we have the following relation [24, 25]:

$$\langle |p_{\text{out}}| \rangle^2 = \langle |j_{\perp y}| \rangle^2 + x_E^2 (\langle |j_{\perp y}| \rangle^2 + 2\langle |k_{\perp y}| \rangle_{\text{parton}}^2), \quad (50)$$

where $\langle |p_{\text{out}}| \rangle$ is the average transverse momentum out of the plane defined by the momentum of the trigger particle $\vec{p}_{\perp, \text{trig}}$ and the beam axis, $j_{\perp y}$ is the component of the particle momentum perpendicular to the jet momentum in the fragmentation process, and $\langle |k_{\perp y}| \rangle_{\text{parton}}^2 = \langle k_{\perp}^2 \rangle_{\text{parton}} / \pi$. On the other hand, partonic $\langle k_{\perp}^2 \rangle_{\text{parton}}$ is related to the transverse momentum imbalance as $\langle q_{\perp}^2 \rangle = 2\langle k_{\perp}^2 \rangle_{\text{parton}}$. Realizing that:

$$\langle |p_{\text{out}}| \rangle = p_{\perp, \text{assoc}} \sin(|\Delta\phi|) = p_{\perp, \text{assoc}} \sin\left(\sqrt{\frac{2}{\pi}} \sigma_F\right), \quad (51)$$

where $p_{\perp, \text{assoc}}$ is the transverse momentum of the associated particle, and

$$x_E = -\frac{\vec{p}_{\perp, \text{assoc}} \cdot \vec{p}_{\perp, \text{trig}}}{p_{\perp, \text{trig}}^2} \approx -\frac{p_{\perp, \text{assoc}}}{p_{\perp, \text{trig}}} \cos(|\Delta\phi|) = -\frac{p_{\perp, \text{assoc}}}{p_{\perp, \text{trig}}} \cos\left(\sqrt{\frac{2}{\pi}} \sigma_F\right), \quad (52)$$

we obtain:

$$\cos^2\left(\sqrt{\frac{2}{\pi}} \sigma_F\right) = \frac{1 - \frac{\langle |j_{\perp y}| \rangle^2}{p_{\perp, \text{assoc}}^2}}{1 + \frac{\langle |j_{\perp y}| \rangle^2}{p_{\perp, \text{trig}}^2} + \frac{1}{\pi} \frac{\langle q_{\perp}^2 \rangle}{p_{\perp, \text{trig}}^2}}. \quad (53)$$

It has been shown that $\langle |j_{\perp y}| \rangle \approx 400 \text{ MeV}$ is sensitive only to vacuum fragmentation and is independent of the center-of-mass energy \sqrt{s} and the trigger particle momentum [24, 25]. Thus, for the selected trigger and associated particles (with specific momenta), the width of the away-side peak σ_F depends closely on the transverse momentum imbalance $\langle q_{\perp}^2 \rangle$.

The PHENIX collaboration at RHIC has measured σ_F , as shown in Fig. 4. We first compute $\Delta\langle q_{\perp}^2 \rangle$ by taking $\xi^2 = 0.12 \text{ GeV}^2$ [7] and by using the CTEQ6L1 parton distribution functions [26] and the deFlorian-Sassot-Stratmann

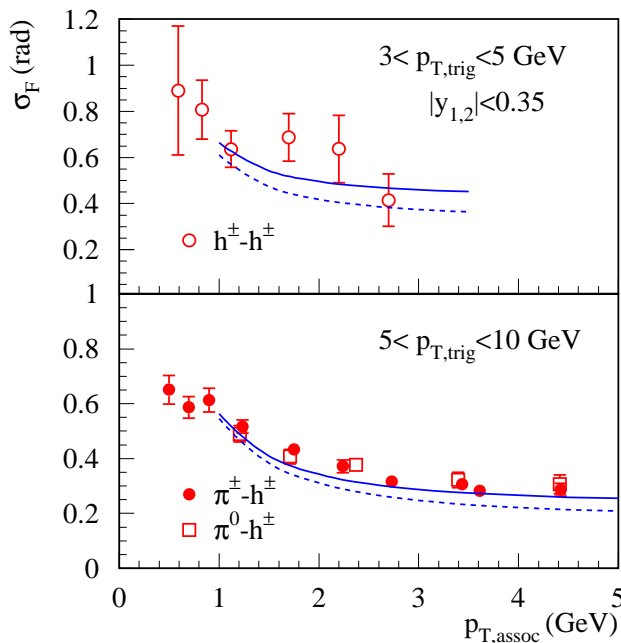


FIG. 4. The width σ_F of the away-side correlation is plotted as a function of the associated hadron transverse momentum $p_{\perp, \text{assoc}}$. Both hadrons are at mid-rapidity $|y_{1,2}| < 0.35$. The upper panel is for $3 < p_{\perp, \text{trig}} < 5$ GeV and the lower panel is for $5 < p_{\perp, \text{trig}} < 10$ GeV. Solid curves represent the width calculated from $\langle q_{\perp}^2 \rangle_{dA} = \langle q_{\perp}^2 \rangle_{pp} + \Delta \langle q_{\perp}^2 \rangle$ and include multiple scattering effect. Dashed are calculated from $\langle q_{\perp}^2 \rangle_{pp}$. Data is from PHENIX [4].

(DSS) hadron fragmentation functions [27]. We choose $\langle q_{\perp}^2 \rangle_{pp} \approx 3.3$ GeV² extracted from PHENIX p+p data [24] to evaluate $\langle q_{\perp}^2 \rangle_{dA}$ in d+Au collisions.

In Fig. 4 the width σ_F of the away-side peak is plotted as a function of the associated particle transverse momentum $p_{\perp, \text{assoc}}$ for two ranges of the trigger particle momentum in the minimum bias d+Au collisions. The solid curves are calculated from $\langle q_{\perp}^2 \rangle_{dA}$, while the dashed ones are from $\langle q_{\perp}^2 \rangle_{pp}$ (i.e., without multiple scattering). Even though the increase in the transverse momentum imbalance $\Delta \langle q_{\perp}^2 \rangle$ is on the order of 2–3 GeV², the broadening effect in the width σ_F is moderate for the mid-mid correlation, where both trigger and associated particles are in the mid-rapidity region $|y_{1,2}| < 0.35$. Nevertheless, the calculated σ_F with multiple scattering effects appears to agree with the PHENIX data slightly better.

B. Nuclear modification factor in d+Au collisions

Coherent multiple parton scattering can also affect the rate of dihadron production. The difference between p+A (d+A) and p+p reactions is usually quantified by the nuclear modification factor:

$$R_{dA}^{(2)} = \frac{d\sigma_{dA}/dy_1 dy_2 dp_{1\perp} dp_{2\perp}}{\langle N_{coll} \rangle d\sigma_{pp}/dy_1 dy_2 dp_{1\perp} dp_{2\perp}}. \quad (54)$$

There are two major effects that control the magnitude of $R_{dA}^{(2)}$: dynamical shadowing [7, 13] and cold nuclear matter energy loss [19, 21, 28]. Dynamical shadowing effects have been shown in Refs. [7, 13] to contribute to the cross section at the power corrections level. Nuclear size enhanced ($A^{1/3}$) power corrections can be resummed for a given partonic channel, as shown by Qiu and Vitev, and lead to the following shift in the momentum fraction x for the parton inside the nucleus (t -channel):

$$x \rightarrow x \left(1 + C_d \frac{\xi^2 (A^{1/3} - 1)}{-\hat{t}} \right), \quad (55)$$

where $C_d = 1$ (C_A/C_F) if parton d is a quark (gluon) in the partonic channel $ab \rightarrow cd$. The reason for the values of C_d is that ξ^2 has been determined for coherent quark scattering [22]. For the hard scattering partons that couple to the nucleus through other channels (c in the u -channel and a in the s -channel), similar shifts in the momentum fraction x have been derived in [13]. These can be obtained easily from Eq. (55) by substituting $\hat{t} \rightarrow \hat{u}$ and $\hat{t} \rightarrow \hat{s}$,

respectively, and by keeping track of the flavor of partons c and a : $C_d \rightarrow C_c$ and $C_d \rightarrow C_a$. In our paper we have taken into account the shift in x consistently for all three channels.

It is important to emphasize the similarities and differences between the dynamical shadowing calculation performed by Qiu and Vitev and the nuclear enhancement in the dijet (dihadron) imbalance presented in our last section. Qiu and Vitev studied the multiple scattering contributions to the dihadron differential cross section directly. These contributions are power suppressed by the hard scale, for example $\propto A^{1/3}\xi^2/\hat{t}$ for the t -channel. In Refs. [7, 13] the coherent multiple scatterings have been resummed and have been shown to lead to the shift in x specified in Eq. (55). When this shift is small, only the first term in the resummed series is important and it is directly proportional to the twist-4 correlation function $T_{q,g/A}^{(I,F)}(x)$. On the other hand, here we calculate the multiple scattering contribution to the q_{\perp}^2 -weighted differential cross section. In the evaluation of the double scattering contribution to this weighted cross section we can set $k_{\perp} = 0$ in the hard parts. Because of the same partonic scattering origin, the dijet imbalance enhancement $\Delta\langle q_{\perp}^2 \rangle$ and the nuclear modification factor $R_{dA}^{(2)}$ depend on the same characteristic scale ξ^2 .

As the parton from the proton undergoes multiple scattering in the nucleus before the hard collisions, it can lose energy due to medium-induced gluon bremsstrahlung. The spectrum of this initial-state energy loss was first derived in [19]. At collider energies, for mid and forward rapidities ($y \geq 0$) even particles of small p_{\perp} come from partons of very high energy in the rest frame of the nucleus (A is at large negative y). In this regime, initial-state cold nuclear matter energy loss can noticeably affect the experimentally measured cross sections [13]. There is renewed interest in constraining its magnitude through measurements with electromagnetic final states, such as the Drell-Yan production [21, 28]. Initial-state energy loss has been implemented in the evaluation of hadronic and jet observables [13, 29, 30]. Such studies build upon early cold nuclear matter energy loss phenomenology [31–34].

For a generic differential cross section, medium-induced radiative corrections factorize from the hard scattering process and enter as an integral convolution. For initial-state energy loss, a simple change of variables presents the effect as a rescaling of the momentum fraction of the incoming parton from the proton [21]:

$$\frac{d\sigma}{dPS} = \int dx' dx \left[\int d\epsilon P(\epsilon) f\left(\frac{x'}{1-\epsilon}\right) \right] f(x) \frac{1}{2x'xs} \langle |\mathcal{M}(x'P', xP)|^2 \rangle (2\pi)^4 \delta^4(p_i - p_f), \quad (56)$$

where $\langle |\mathcal{M}(x'P', xP)|^2 \rangle = H_{ab \rightarrow cd}^U(\hat{s}, \hat{t}, \hat{u})$ defined in Sec. II. For a single ($n_g = 1$) emitted gluon $dN^g(\epsilon)/d\epsilon = P(\epsilon)$ is the probability distribution for fractional energy loss ϵ . In general, $n_g \neq 1$ and the probability distributions $P_{q,g}(\epsilon)$ is constricted from $dN^g(\epsilon)/d\epsilon$ in the independent Poisson approximation, $\epsilon = \sum_i \omega_i/E$. In the soft gluon approximation medium-induced radiative corrections always factorize from the hard short-distance scattering [19, 35]. For arbitrary kinematics, this factorization is always exact for parent quarks [35]. Just like in the vacuum, beyond the soft gluon approximation medium-induced splitting kernels for parent gluons factorize only for polarization-averaged observables [20]. In this manuscript we work in the soft medium-induced splitting approximation which allows for an energy loss interpretation of the cross section suppression. From Eq. (56), this effect is easily implemented through:

$$f_{q,\bar{q}}(x') \rightarrow \int_0^1 d\epsilon P_q(\epsilon) f_{q,\bar{q}}\left(\frac{x'}{1-\epsilon}\right), \quad f_g(x') \rightarrow \int_0^1 d\epsilon P_g(\epsilon) f_g\left(\frac{x'}{1-\epsilon}\right). \quad (57)$$

In Fig. 5, we plot the nuclear modification factor $R_{dA}^{(2)}$ in d+Au collisions for dihadron production as a function of mean binary collision number $\langle N_{\text{coll}} \rangle$ for both mid-forward (top panel) and forward-forward (bottom panel) correlated pairs. To take into account the centrality dependence, in both the transverse momentum imbalance and the dynamical shadowing we have replaced $A^{1/3} \rightarrow A^{1/3} \langle N_{\text{coll}}^{dA}(b) \rangle / \langle N_{\text{coll}}^{dA}(b_{\text{min}, \text{bias}}) \rangle$ [7]. In the calculation of initial-state radiative energy loss [19, 21] the average length of the medium is similarly scaled. For both mid-forward and forward-forward cases, the associated particles are in the forward-rapidity region $3.0 < y_2 < 3.8$ with momenta $1.0 < p_{\perp, \text{assoc}} < 1.5$ GeV. For the mid-forward case the trigger particle is at mid-rapidity $|y_1| < 0.35$, while for the forward-forward case the trigger particle is at forward rapidity $3.0 < y_1 < 3.8$. The solid curves contain both dynamical shadowing and energy loss effects, whereas the dashed curves contain only the dynamical shadowing effect. As we can see, the calculated $R_{dA}^{(2)}$ give a very good description for the mid-forward correlated pairs. The current experimental data still has large uncertainties, and is not able to further constrain the individual contribution of dynamic shadowing and the cold nuclear matter energy loss. For the forward-forward correlated pairs our formalism is still roughly consistent with the PHENIX measurements [5], though the agreements get slightly worse. In particular, for the most-central collisions the data seems to indicate a very strong suppression. Initial-state energy loss plays an important role in bringing the calculation closer to the data, as it does for inclusive particle production at forward rapidities [21]. It will be interesting to see whether such suppression factor can be explained within other formalisms, for example those based on color glass condensate [8, 9].

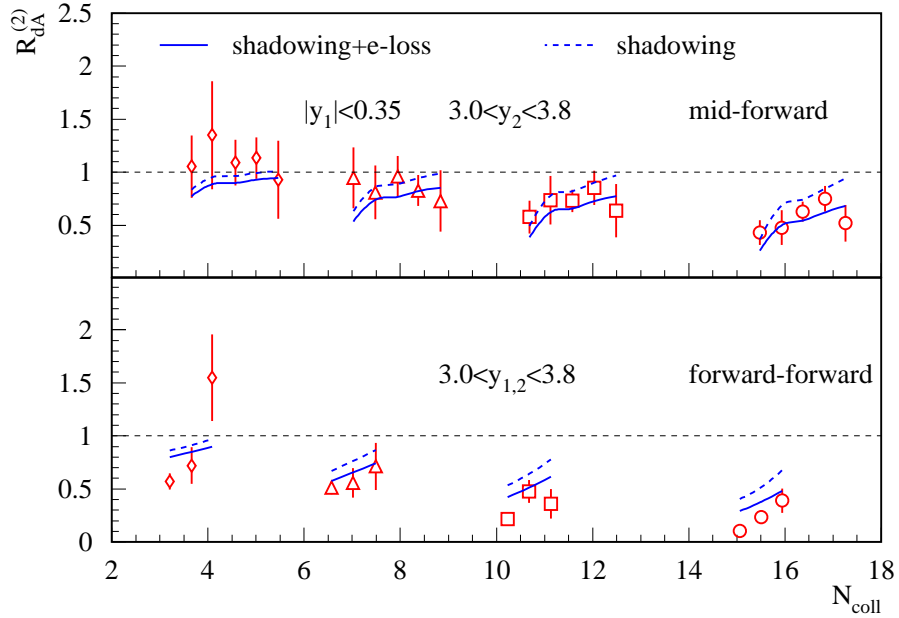


FIG. 5. Nuclear modification factor $R_{dA}^{(2)}$ for back-to-back dihadron production in d+Au collisions. Solid curves contain both dynamical shadowing and energy loss effect, whereas dashed curves contain only dynamical shadowing. Both top and bottom panels have an associated particle in the forward-rapidity $3.0 < y_2 < 3.8$ and $1.0 < p_{\perp, \text{assoc}} < 1.5$ GeV region. From left to right there are four groups corresponding to a mean binary collision number $\langle N_{\text{coll}} \rangle = 3.2, 6.6, 10.2,$ and 15.1 , respectively, even though they have been offset from these actual values for visual clarity. Top panel: trigger particle at mid-rapidity $|y_1| < 0.35$. Within each centrality selection, from left to right, the transverse momentum of the trigger particle is in the $[1, 2], [2, 4], [2.5, 3], [3, 4],$ and $[4, 7]$ GeV interval. Bottom panel: trigger particle at forward rapidity $3.0 < y_1 < 3.8$. Within each centrality selection, from left to right, the transverse momentum of the trigger particle is in the $[1.1, 1.6], [1.6, 2.0],$ and $[2.0, 5.0]$ GeV interval. Data is from PHENIX [5].

C. Dihadron azimuthal correlations

It is also useful to present directly the dihadron azimuthal correlation distribution, see for example the STAR measurement in Fig. 6. In this case, the dihadron correlation can usually be approximated by two Gaussians for the near-side and the away-side, and a constant background:

$$CP(\Delta\phi) = \frac{1}{N_{\text{norm}}} \frac{dN^{h_1 h_2}}{d\Delta\phi} \approx B + \frac{A_N}{\sqrt{2\pi}\sigma_N} \exp\left\{-\frac{\Delta\phi^2}{2\sigma_N^2}\right\} + \frac{A_F}{\sqrt{2\pi}\sigma_F} \exp\left\{-\frac{(\Delta\phi - \pi)^2}{2\sigma_F^2}\right\}. \quad (58)$$

If we concentrate on the away-side peak, the area under the Gaussian peak A_F is proportional to the production rate for approximately back-to-back hadron pairs. In going from p+p to d+Au collisions, we thus have:

$$R_{dA}^{(2)} = \frac{A_F^{dAu}}{A_F^{pp}}. \quad (59)$$

If one knows A_F^{pp} for p+p collisions, from the theoretically calculated $R_{dA}^{(2)}$ in the last subsection, one can predict the area under the Gaussian peak A_F^{dAu} in d+Au collisions.

On the other hand, the width σ_F of the away-side peak can be determined from the transverse momentum imbalance through Eq. (53). The change from p+p to d+Au will mainly depend on $\Delta\langle q_{\perp}^2 \rangle$, which can be calculated in our formalism from Eq. (47). To obtain the dihadron azimuthal correlation in d+Au collisions, we first fit the dihadron correlation in p+p collisions to obtain A_F^{pp} and σ_F^{pp} . We get:

$$B = 0.0051, \quad A_N = 0.0122, \quad \sigma_N = 0.4238, \quad A_F = 0.0159, \quad \sigma_F = 0.7135. \quad (60)$$

From Eq. (53), using $\langle p_{1\perp} \rangle \sim 2.54$ GeV and $\langle p_{2\perp} \rangle \sim 1.28$ GeV in p+p collision [36], we find $\langle q_{\perp}^2 \rangle_{pp} \sim 5.0$ GeV². We then calculate $\langle q_{\perp}^2 \rangle_{dAu} = \langle q_{\perp}^2 \rangle_{pp} + \Delta\langle q_{\perp}^2 \rangle$ to obtain the away-side width σ_F in d+Au collisions. On the other hand, with our calculation of $R_{dA}^{(2)}$ we get A_F^{dAu} from Eq. (59). The dihadron azimuthal correlations obtained this way are compared to the STAR experimental data [6] for both central and peripheral collisions in Fig. 6. The solid curves are

calculated with $R_{dA}^{(2)}$ containing both dynamical shadowing and cold nuclear matter energy loss effects. The dashed curves are calculated with only dynamical shadowing. The constant offset is $B = 0.01405$ for central collisions and $B = 0.0066$ for peripheral collisions. As we can see from the plot, our calculation gives a very good description of the experimental data in central collisions. For peripheral collisions, the agreements get worse. The main reason for the deviation comes from the fact that the experimental data for peripheral d+Au collisions show a clear broadening effect in the away-side width σ_F [6]. However, our calculated broadening $\Delta\langle q_{\perp}^2 \rangle_{dAu} \propto A^{1/3} \langle N_{\text{coll}}^{dA}(b) \rangle / \langle N_{\text{coll}}^{dA}(b_{\text{min.bias}}) \rangle$ becomes quite small.

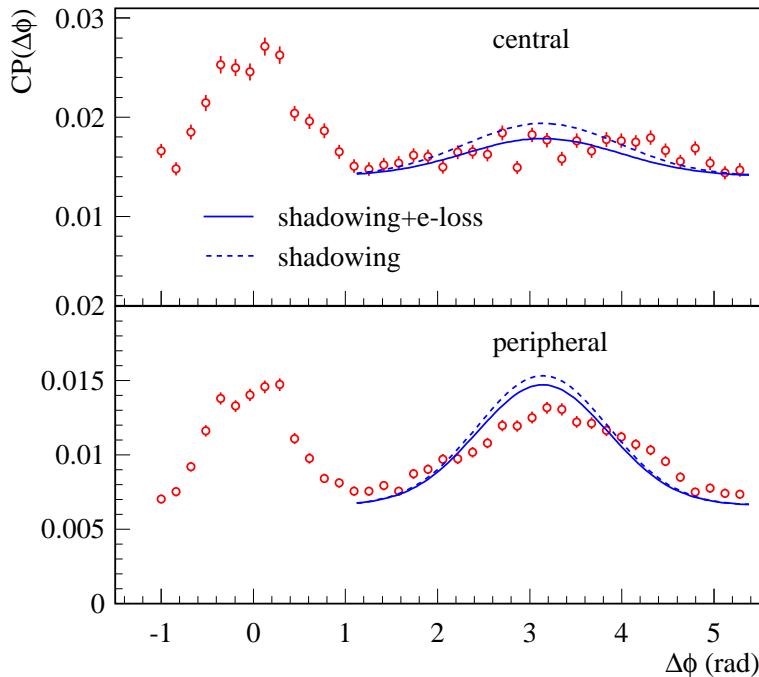


FIG. 6. Azimuthal correlation associated with back-to-back dihadron production in central (top) and peripheral (bottom) d+Au collisions. Theoretical curves are calculated for $\langle y_1 \rangle = \langle y_2 \rangle = 3.2$ and $\langle p_{1\perp} \rangle = 2.68$ GeV and $\langle p_{2\perp} \rangle = 1.31$ GeV in d+Au collision [36]. Data is from STAR [6].

IV. CONCLUSIONS

In summary, by taking into account both initial- and final-state multiple parton scattering inside the nucleus, we calculated in perturbative QCD the increase in the transverse momentum imbalance (nuclear-induced broadening) of dijet and dihadron production in high energy p+A (d+A) collisions relative to the more elementary p+p collisions. The nuclear-induced broadening can be used to calculate the width of the away-side peak in dihadron correlation measurements. For phenomenological applications, we combined our new theoretical findings with previously derived coherent power correction (dynamical shadowing) and cold nuclear matter energy loss results. Perturbative QCD calculations that take these effects into account were recently shown to give a good description of forward rapidity single inclusive particle production in d+Au collision at RHIC. In this manuscript we provided the corresponding evaluation for dihadron cross sections and correlations relevant to the new STAR and PHENIX measurements. With cold nuclear matter parameters constrained by data on deep inelastic scattering on nuclei, we found that the calculated nuclear modification factor is roughly consistent with the PHENIX experimental data. Finally, by combining the calculated width of the away-side peak and the nuclear suppression factor, we were able to describe reasonably well the dihadron azimuthal correlations measured by the STAR experiment. Even though we need the baseline from p+p collisions, our formalism does describe the effects of cold nuclear matter in going from p+p to d+Au collisions pretty well for mid-mid, mid-forward, and forward-forward correlated hadron pairs at RHIC.

ACKNOWLEDGMENTS

We thank L. Bland, E. Braidot, A. Ogawa, and X. Li for helpful correspondence on the STAR experimental data, and B. Meredith for the helpful correspondence on the PHENIX experimental data. This research is supported by the US Department of Energy, Office of Science, under Contract No. DE-AC52-06NA25396 and DE-AC02-98CH10886, and in part by the LDRD program at LANL, NSFC of China under Projects Nos. 10825523 and 10875025.

-
- [1] D. Boer *et al.*, arXiv:1108.1713 [nucl-th]; C. A. Salgado *et al.*, arXiv:1105.3919 [hep-ph]; C. Marquet, arXiv:1101.3466 [hep-ph]; Z. -B. Kang and F. Yuan, Phys. Rev. D **84**, 034019 (2011) [arXiv:1106.1375 [hep-ph]].
- [2] I. Arsene *et al.* [BRAHMS Collaboration], Phys. Rev. Lett. **93**, 242303 (2004) [nucl-ex/0403005].
- [3] S. S. Adler *et al.* [PHENIX Collaboration], Phys. Rev. Lett. **94**, 082302 (2005) [nucl-ex/0411054].
- [4] S. S. Adler *et al.* [PHENIX Collaboration], Phys. Rev. C **73**, 054903 (2006) [nucl-ex/0510021].
- [5] A. Adare *et al.* [PHENIX Collaboration], Phys. Rev. Lett. **107**, 172301 (2011) [arXiv:1105.5112 [nucl-ex]].
- [6] E. Braidot [STAR Collaboration], Nucl. Phys. A **854**, 168 (2011) [arXiv:1008.3989 [nucl-ex]]; E. Braidot, arXiv:1102.0931 [nucl-ex].
- [7] J. -W. Qiu and I. Vitev, Phys. Lett. B **632**, 507 (2006) [hep-ph/0405068].
- [8] J. L. Albacete and C. Marquet, Phys. Rev. Lett. **105**, 162301 (2010) [arXiv:1005.4065 [hep-ph]].
- [9] A. Stasto, B. -W. Xiao and F. Yuan, arXiv:1109.1817 [hep-ph].
- [10] M. Strikman and W. Vogelsang, Phys. Rev. D **83**, 034029 (2011) [arXiv:1009.6123 [hep-ph]].
- [11] J. Jalilian-Marian and A. H. Rezaeian, arXiv:1110.2810 [hep-ph].
- [12] See, for example: M. Gyulassy, P. Levai and I. Vitev, Nucl. Phys. B **594**, 371 (2001) [nucl-th/0006010]; Y. He, I. Vitev and B. -W. Zhang, arXiv:1105.2566 [hep-ph]; Z. -B. Kang and I. Vitev, Phys. Rev. D **84**, 014034 (2011) [arXiv:1106.1493 [hep-ph]].
- [13] I. Vitev, J. T. Goldman, M. B. Johnson and J. W. Qiu, Phys. Rev. D **74**, 054010 (2006) [hep-ph/0605200].
- [14] C. Marquet, Nucl. Phys. A **796**, 41 (2007) [arXiv:0708.0231 [hep-ph]].
- [15] Z. -B. Kang and J. -W. Qiu, J. Phys. G G **34**, S607 (2007) [hep-ph/0702040 [HEP-PH]].
- [16] Z. -B. Kang and J. -W. Qiu, Phys. Rev. D **77**, 114027 (2008) [arXiv:0802.2904 [hep-ph]].
- [17] M. Luo, J. -W. Qiu and G. F. Sterman, Phys. Rev. D **49**, 4493 (1994); X. -f. Guo, Phys. Rev. D **58**, 114033 (1998) [hep-ph/9804234].
- [18] R. J. Fries, Phys. Rev. D **68**, 074013 (2003) [hep-ph/0209275].
- [19] I. Vitev, Phys. Rev. C **75**, 064906 (2007) [hep-ph/0703002].
- [20] G. Ovanessian and I. Vitev, arXiv:1109.5619 [hep-ph].
- [21] R. B. Neufeld, I. Vitev and B. -W. Zhang, Phys. Lett. B **704**, 590 (2011) [arXiv:1010.3708 [hep-ph]].
- [22] J. -W. Qiu and I. Vitev, Phys. Rev. Lett. **93**, 262301 (2004) [hep-ph/0309094].
- [23] J. F. Owens, Rev. Mod. Phys. **59**, 465 (1987); Z. -B. Kang and F. Yuan, Phys. Rev. D **81**, 054007 (2010) [arXiv:1001.0247 [hep-ph]].
- [24] J. Rak [PHENIX Collaboration], nucl-ex/0306031.
- [25] A. L. S. Angelis *et al.* [CERN-Columbia-Oxford-Rockefeller and CCOR Collaborations], Phys. Lett. B **97**, 163 (1980).
- [26] J. Pumplin, D. R. Stump, J. Huston, H. L. Lai, P. M. Nadolsky and W. K. Tung, JHEP **0207**, 012 (2002) [arXiv:hep-ph/0201195].
- [27] D. de Florian, R. Sassot and M. Stratmann, Phys. Rev. D **75**, 114010 (2007) [hep-ph/0703242 [HEP-PH]].
- [28] H. Xing, Y. Guo, E. Wang and X. -N. Wang, arXiv:1110.1903 [hep-ph].
- [29] R. Sharma, I. Vitev and B. -W. Zhang, Phys. Rev. C **80**, 054902 (2009) [arXiv:0904.0032 [hep-ph]].
- [30] I. Vitev and B. -W. Zhang, Phys. Rev. Lett. **104**, 132001 (2010) [arXiv:0910.1090 [hep-ph]].
- [31] S. Gavin and J. Milana, Phys. Rev. Lett. **68**, 1834 (1992).
- [32] R. Vogt, Phys. Rev. C **61**, 035203 (2000) [hep-ph/9907317].
- [33] M. B. Johnson *et al.* [FNAL E772 Collaboration], Phys. Rev. Lett. **86**, 4483 (2001) [hep-ex/0010051].
- [34] F. Arleo, Phys. Lett. B **532**, 231 (2002) [hep-ph/0201066].
- [35] G. Ovanessian and I. Vitev, JHEP **1106**, 080 (2011) [arXiv:1103.1074 [hep-ph]].
- [36] We thank Les Bland and Ermes Braidot for providing the average value of the transverse momentum $\langle p_{1,2\perp} \rangle$.